ASTENA: A mission concept for a deep study of the transient gamma-ray sky and for nuclear astrophysics

E. Virgilli[1,2,*], F. Frontera[1,3], P. Rosati[1,3,4], C. Guidorzi[1,3,4], L. Ferro[3], M. Moita[3], M. Orlandini[1], F. Fuschino[1,2], R. Campana[1,2], C. Labanti[1], E. Marchesini[1], E. Caroli[1], N. Auricchio[1], J. B. Stephen[1], C. Ferrari[5], S. Squerzanti[4], S. Del Sordo[6], C. Gargano[6] and M. Pucci[7]
on behalf of the ASTENA Collaboration

[1] *INAF - OAS di Bologna, Via Piero Gobetti 93/3, I-40129 Bologna, Italy*
[2] *INFN Sezione di Bologna Viale C. Berti Pichat, 6/2 – 40127 Bologna, Italy*
[3] *Dept. of Physics and Earth Science, Univ. of Ferrara, Via Saragat 1, I-44122, Ferrara, Italy*
[4] *Istituto Nazionale di Fisica Nucleare, INFN-Sezione di Ferrara, 44122 Ferrara, Italy*
[5] *CNR-IMEM Institute, Parco Area delle Scienze 37/A, 43124 Parma, Italy*
[6] *INAF/IASF-Palermo, Via Ugo La Malfa 153, 90146 Palermo, Italy*
[7] *CNR - Istituto Nazionale di Ottica - Largo Fermi 6, 50125 Firenze, Italy*
[*] *E-mail: enrico.virgilli@inaf.it*

Gamma-ray astronomy is a branch whose potential has not yet been fully exploited. The observations of elemental and isotopic abundances in supernova (SN) explosions are key probes not only of the stellar structure and evolution but also for understanding the physics that makes Type-Ia SNe as standard candles for the study of the Universe expansion properties. In spite of its crucial role, nuclear astrophysics remains a poorly explored field mainly for the typical emission lines intensity which are vanishing small and requires very high sensitivities of the telescopes. Furthermore, in spite that the Galactic bulge-dominated intensity of positron annihilation line at 511 keV has been measured, its origin is still a mystery due to the poor angular resolution and insufficient sensitivity of the commonly employed instrumentation in the sub-MeV energy domain. To answer these scientific issues a jump in sensitivity and angular resolution with respect to the present instrumentation is required. Conceived within the EU project AHEAD, a new high energy mission, capable of tackling the previously mentioned topics, has been proposed. This concept of mission named ASTENA (Advanced Surveyor of Transient Events and Nuclear Astrophysics), includes two instruments: a Wide Field Monitor with Imaging and Spectroscopic (WFM-IS, 2 keV - 20 MeV) capabilities and a Narrow Field Telescope (NFT, 50 - 700 keV). Thanks to the combination of angular resolution, sensitivity and large FoV, ASTENA will be a breakthrough in the hard X and soft gamma–ray energy band, also enabling polarimetry in this energy band. In this talk the science goals of the mission are discussed, the payload configuration is described and expected performances in observing key targets are shown.

Keywords: Soft gamma-rays; hard x-ray telescope; Focusing gamma rays; Bragg diffraction; bent crystals.

1. Introduction

Within the H2020 European program AHEAD,[1,2] (integrated Activities for High Energy Astrophysics Domain) devoted to the assessment of future gamma-ray experiments, a Scientific Advisory Group recommended the prime scientific questions that might be addressed by a future space mission operating in the gamma-ray energy domain. The high-priorities themes resulted to be the nuclear astrophysics and

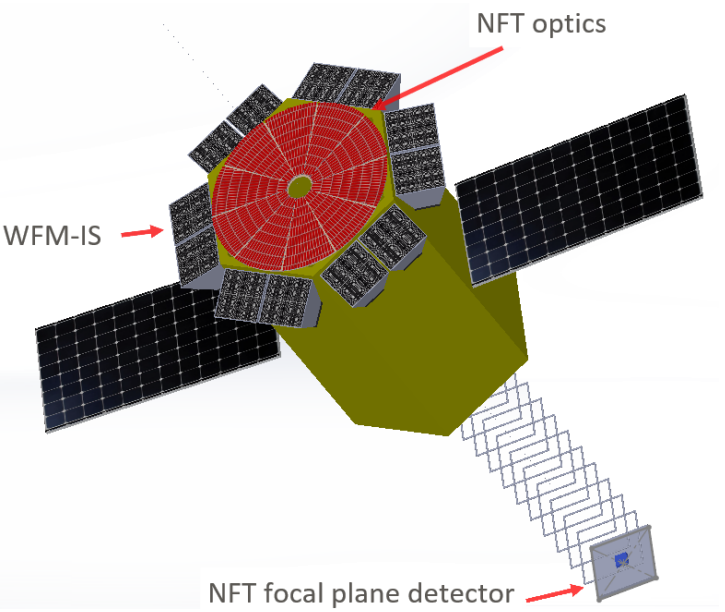

Fig. 1. Drawing of the ASTENA mission. The NFT (in red) is a 20 m focal length Laue lens made with bent Germanium and Silicon crystals. At the focal distance is positioned a focal plane detector (blue) which is a solid state device made with 4 layers of Cadmium Zinc Telluride. The focal distance is achieved through a deployable mast which at launch is fully enclosed in the spacecraft and in operative condition extends from the bottom of the spacecraft for 15 m, which is a reasonable distance for the stability of an extendable structure. The WFM-IS composed of 12 Position Sensitive Detectors (PSDs) distributed around the NFT and oriented 15 degrees two by two outwards with respect to the Laue lens axis in order to extend the FoV of the overall instrument.

the study of the transient sky. According to those themes, the ASTENA (Advanced Surveyor for Transient Events and Nuclear Astrophysics) has been designed. The ASTENA concept mission, which is shown in Fig. 1, is a broad energy pass-band experiment composed by two complementary instruments. The first is a Wide Field Monitor with Imaging and Spectrometric capabilities (WFM-IS) with an outstanding broad energy pass-band from 2 keV to 20 MeV. It consists on 12 coded mask cameras deployed in a circular pattern around the hexagonal spacecraft and oriented at 15 degrees with respect to the spacecraft axis. The overall Field of View (FoV) of the instrument is $\sim$2 steradians. The second instrument is a narrow FoV (few arcminutes) telescope based on a Laue lens with a geometric area of $\sim$7 m^2 and 20 m focal length, capable to focus photons in the broad energy pass-band 50 - 700 keV on a solid state detector. The Narrow Field Telescope (NFT) represents a technological breakthrough as its optics, based on the diffraction from bent crystals, provides an unprecedented sensitivity with respect to any other mission flown and operative in the same energy pass-band. At launch, we expect to keep the WFM-IS cameras and the focal plane detector stored within the cylindrical spacecraft

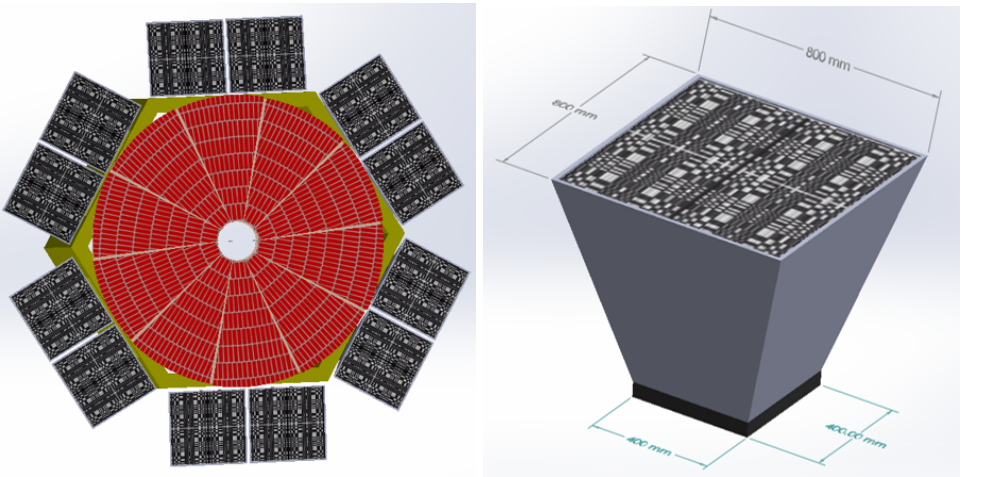

Fig. 2. Left: Top view of the instruments on board ASTENA. The 12 PSD of the WFM/IS are coupled 2 by two and are positioned around the hexagonal structure of the spacecraft. Each PSD is surmounted by a coded mask which ensures the imaging capability up to 150 keV. The red part is the broad energy pass-band Laue with 15 m focal length. Right: Detail of one PSD in which is visible the coded mask and the collimator surrounding the instrument. At the bottom (dark profile) is visible the detection plane made with scintillator bars which are coupled with SDDs (see text for the explanation of the instrument working principle).

whose diameter is 1.5 m and the length is 5 m. In the operational configuration an extendable boom brings the focal plane detector 15 m apart from the bottom of the spacecraft while a mechanism discloses and tilts the coded mask cameras at their nominal position and angle. In the following currently on-going project called AHEAD2020 the mission concept is being refined and optimized. The mission has been proposed in the ESA call "Voyage 2050"[3] as a future medium class mission for hard X-/soft gamma-ray astrophysics.[4,5] The final recommendation of the Senior Committee has confirmed the key importance of the high energy observations from space with high sensitivity and capable of enabling spectro-polarimetry based on new technologies, particularly in synergy with gravitational wave astronomy for resolving some of the fundamental questions still unanswered in astrophysics related to the nucleosynthesis in explosive events or to the accretion mechanism on compact sources.

2. The ASTENA configuration

The ASTENA mission concept builds on the complementarity between the two instruments on board. The WFM-IS is composed by 12 coded mask cameras equipped with Position Sensitive Detectors (visible in Fig.2 - left) (PSDs) distributed two by two around the hexagonal spacecraft envelope. Each pair of PSDs in the same hexagon side is co-aligned and directed towards the same direction which is radially tilted outwards of 15 degrees with respect to the satellite axis. Each PSD has a size

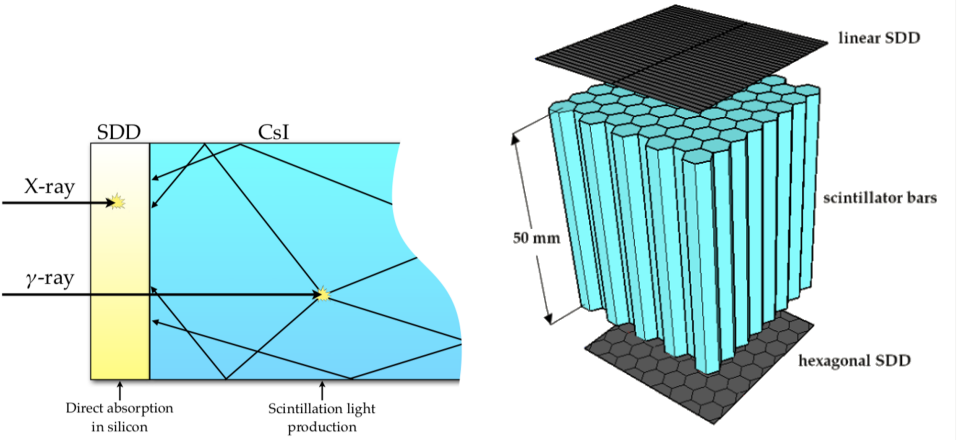

Fig. 3. Left: working principle of the WFM-IS. An hexagonal scintillator bar (cyan) is coupled at both ends (only one end is visible in the picture) with an SDD (yellow). The low energy radiation (< 30 keV) is directly absorbed in the SDD while higher energy photons pass through the SDD and interact in the scintillator bar. The scintillation light, which is produced at some distance from the surface of the scintillator bar and is reflected by the lateral surfaces, is collected by the two SDDs. The comparison between the two signals allows for the determination of the depth of interaction. Right: disposition of the scintillator bars (cyan) and of the top and bottom SDDs (grey). The top SDD is equipped with an array of linear anodes therefore the charge collected provides information only in one direction. In the bottom SDD the anodic structure has a hexagonal shape in order to fully exploit this geometry which minimizes the directional bias for polarimetric measurements, if compared with a detector with square (cubic) pixelization (voxelization).

of 43×42 cm^2 and is made of ~ 6500 scintillator bars with hexagonal cross section (5 mm between flat sides) and 50 mm long. Both ends of the scintillator bars are optically coupled with two Silicon Drift Detectors (SDDs) 400 μm thick. The instrument is based on the same detection principle of the X and Gamma-ray Imager and Spectrometer (XGIS) on board the THESEUS mission[6] which was proposed as 5^{th} medium-class mission for the ESA Cosmic Vision Programme (M5).

The detection principle (see Fig. 3) is based on a different interaction of the radiation with the system, depending on the energy of the interacting photons. Low energy photons (< 30 keV) are directly absorbed in the SDD while photons with higher energy pass through the SDD and interact in the scintillator bar. The scintillation light, which is produced at some distance from the ends of the scintillator bars, is reflected by the lateral surfaces which are properly polished and wrapped in order to reflect as much as possible the light produced, and it is collected by the two SDDs optically coupled at both ends of the bar. For high energy photons (>30 keV) the detector is position sensitive with a 3-D resolution given that the position of interaction of the gamma-ray photon along the bar can be reconstructed by comparing the signal collected from the two opposed SDDs. The top SDDs (those facing the sky) have the dual purpose of directly detecting the low energy photons (below few tens of keV) and of collecting the scintillation light emitted

by the scintillator bar when photons with higher energy pass through them. They have a linear anodic structure therefore are sensitive only to one direction (X or Y) with spatial resolution of 1.25 mm. Given that each pair of PSDs placed at the same side of the spacecraft have perpendicular anodes, they behave like a 2-D detector. Instead, the bottom SDD has hexagonal shape and it is used to get the 3-D position sensitivity. In this way we can minimize the background through the Compton kinematics reconstruction of the trajectory of the photons and exploit the polarimetric capability of the instrument. Different scintillator materials as Cesium Iodide (CsI(Tl)), Gadolinium Aluminium Gallium Garnet (GAGG), Lutetium Yttrium Orthosilicate (LYSO(Ce)) are under investigation in order to find the optimal properties to fit the instrument requirements. Each PSD is surmounted by a double scale[7] square coded mask with side of 80 cm at a distance of 70 cm from the detector plane (see Fig. 2 - right). The double scale enables imaging with Point Source Location Accuracy (PSLA) of 1 arcmin for a 7σ signal for photons with energy < 30 keV and PSLA of 5 arcmin for photons in the energy range 30 - 150 keV. In Fig. 4 (left) the PSLA as a function of the significance of the observation for different configurations of the WFM-IS is reported, compared with required PSLA of 1 arcminute. In Fig. 4 (right) the integrated sensitivity of the overall WFM-IS is reported as a function of the integration time, divided in three relevant pass-bands according to the different detection principle employed (2 - 10 keV: direct detection in the SDDs, 30 - 150 keV: interaction with the scintillator bars, 150 keV - 10 MeV: uncollimated interaction in the scintillator bar). Above 150 keV the coded mask is transparent to radiation and an effective imaging capability can be enabled through two features: 1. by exploiting the Compton kinematics for the photon direction reconstruction and 2. by taking advantage of the different measured photon intensity from the 6 blocks which are - in general - differently oriented with respect to the direction of the observed event, except for perfectly on-axis sources. With these configuration the instrument can provide a FoV of $\sim$2 sr with an angular resolution of a few arcmin and an unprecedented energy pass-band of 2 keV - 20 MeV which has never been achieved so far with a single device.

The second instrument is a 20 m long focal length Laue lens based on bent crystals made with Germanium and Silicon. The crystals are distributed in 43 concentric rings and, according to the spherical geometry and to the Bragg law, the lower energies are reflected from outer rings while inner rings are responsible for focusing the higher energies. The size of the crystals have been chosen to be 30×10 mm^2, the longer dimension being the focusing direction. In the other direction, no concentration is expected due to the cylindrical curvature of the tiles. The cross section of the tiles has been chosen in order to tile the overall geometric area with a moderate number of crystals ($\sim$19500) by minimizing the amount of uncovered area (the optics filling factor results above 85%). Depending on the energy to be diffracted the crystal thickness is optimized in order to maximize the diffraction efficiency. For both materials the 111 planes are assumed in order to exploit the

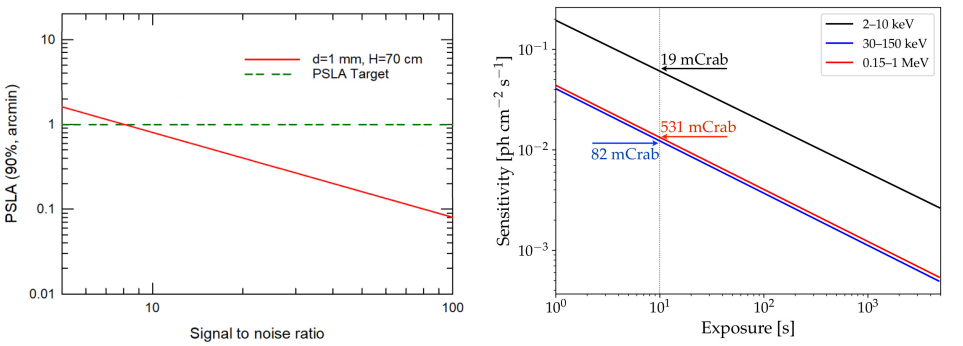

Fig. 4. Left: Point Source Location Accuracy (PSLA) for the WFM-IS as a function of the signal to noise ratio. The parameter d is the distance between the anodes of the top SDDs. The requird PSLA is also shown (green dashed line) Right: Integrated continuum sensitivity expressed in photons/cm^2/s as a function of the exposure time for the three significant energy pass-bands acquired for direct absorption in the SDDs (black curve, 2 - 10 keV), through the scintillation bars (30 - 150 keV, blue curve) and as a Compton detector with no coded mask (150 keV - 1 MeV, red curve).

so called secondary curvature of the diffraction planes induced in crystals for some crystallographic orientation (including the 111) allowing to achieve a throughput which overcomes the limitation of the 50% of the incident beam, which is the limit of mosaic and flat perfect crystals.

Orders of diffraction higher than the fundamental are being considered in the simulations in order to maximize the effective area, particularly in the energy range 500 - 520 keV (at the expenses of the effective area at lower energies) in order to increase the sensitivity at the energy of interest for the detection of the weak e^+/e^- annihilation line from the Galactic center (see Sect. 3 for further details). At 20 m from the optics is placed the focal plane detector which is kept at the correct position with a deployable mast. The detector is made with 4 layers of Cadmium Zinc Telluride (CZT) with cross section 80 $\times$ 80 mm^2 each with a thickness of 20 mm. The detector has a 3-D spatial resolution of about 300 μm in all directions. This is achievable with a proper disposition of the anodes on the top and bottom of each CZT layer. Thanks to the overall detector thickness its detection efficiency is greater than 80% at 600 keV with energy resolution of 1% at 511 keV.

The NFT continuum sensitivity which has been derived at Low Earth Orbit (LEO) by comparison with the background measured by the Spectrometer on-board INTEGRAL SPI[8] is reported in Fig. 6 (top). The curve has been estimated for an integration time of 10^5 s and at 3σ confidence level. For comparison, in the plot has been reported a number of past and present experiments exploiting the direct view principle (equipped with coded masks or collimators) or using focusing telescopes. The energy band in which it is estimated is $\Delta E = E/2$, except in the band from 50 keV to 62.5 keV, in which the energy band linearly increases from $\Delta E = E/4$ to $\Delta E = E/2$, due to the absence of crystals diffracting energies

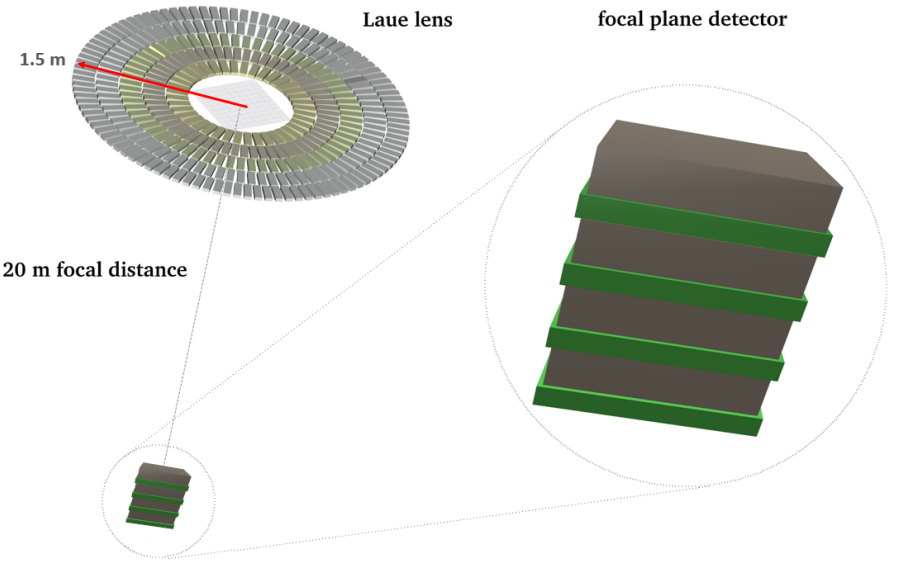

Fig. 5. Left: The optics of the NFT composed by 43 rings of crystal tiles made with Silicon and Germanium. The optics has a radius of 1.5 m for a total geometric area of about 7 m^2. At 20 m from the Laue lens is placed the focal plane detector. Right: a Geant4 drawing of the main components of the focal plane detector which is made of 4 layers of a solid state Cadmium Zinc Telluride (CZT, dark grey) with 3-D spatial resolution, spectral and polarimetric capabilities.

below 50 keV. Uncertainties in the realization of the optics have been also taken into account. The curvature radius of the crystals have been considered within 5% of the nominal radius and the mounting accuracy of about 10 arcseconds with respect to the nominal positioning. The presence of such deviations from the nominal lens realization requirements have effects on the size of the PSF and, ultimately, on the focusing power of the Laue lens. This unprecedented sensitivity is achieved thanks to the use of bent crystals with optimized thickness. Figure 6 (bottom) shows the sensitivity at measuring the flux of emission lines, at 3σ confidence level and for 10^5 s integration time. An intrinsic FWHM of 2 keV has been considered for the lines (e.g. see [9] for the 158 keV line from SN2014J). The narrow line sensitivity is about 1 order of magnitude better than SPI on board INTEGRAL at 511 keV. These values of sensitivities are mainly due to the use of bent crystals, to the transmission geometry and to the focal length that allows for an unprecedented large collecting area.

Laue optics have the great advantage of drastically reducing the instrumental background as the photons are mainly collected into an area of a few mm^2. The drawback is that, as far as the source moves out of the focal axis, the diffracted image spreads over a larger area generating ring-shaped images for coma aberrations. Through ray-tracing and Monte Carlo simulations it has been estimated that,

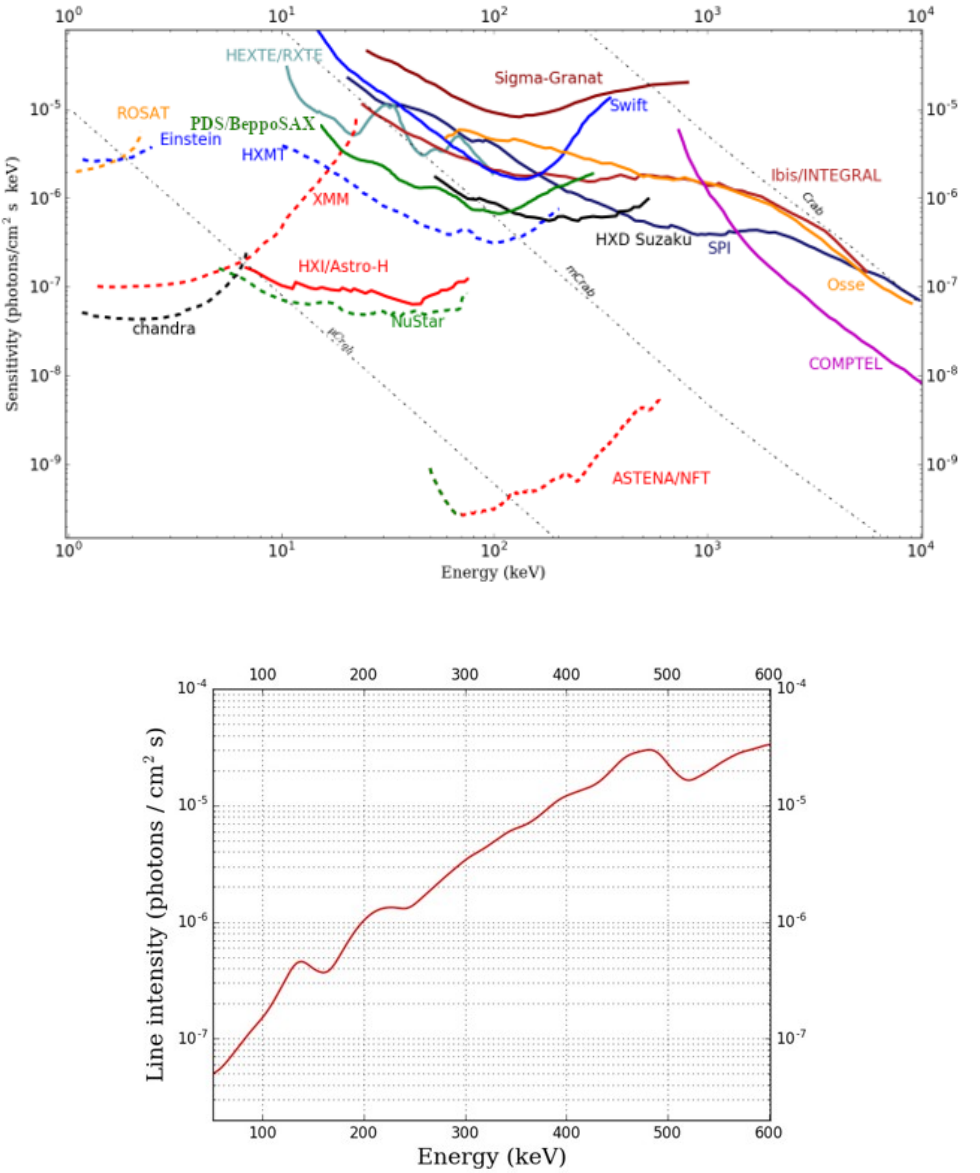

Fig. 6. Top: NFT continuum sensitivity at 3σ confidence level and in 10^5 s of observation time, with $\Delta E = E/2$, except in the band 50 to 62.5 keV, where ΔE linearly increases from $\Delta E = E/4$ to $\Delta E = E/2$, compared with the sensitivity at the same significance and with the same integration time of other missions or experiments (dashed lines represent other focusing experiment, continuum curves correspond to direct view instruments). Bottom: Expected line sensitivity for the NFT, calculated for an integration time of 10^5 s, at 3σ confidence level.

with the defined optics dimension and crystal size, photons from off-axis sources (>4 arcmin) are scattered into a broad detection area.[10] This reduces the benefits of the focusing process. Therefore the FOV of the NFT has been fitted with the PSLA of the WFM-IS in order to exploit the sensitivity of the former for nearly on-axis sources with the excellent broad-band survey capabilities of the latter.

3. Key science with ASTENA

For some relevant scientific key subjects that can be tackled with the instruments on board ASTENA see [10, 11]. Here we summarize these subjects. As mentioned in Sect. 1 the main objectives of the ASTENA mission concept are mainly two. First, ASTENA intends to investigate the intriguing key questions related to the gamma-ray lines in astrophysics. Furthermore, the high sensitivity of the on board instruments joined with the large pass-band of the WFM-IS and their polarimetric capabilities would make ASTENA an ideal tool for shading light in the transient sky, providing also an important contributions to the multi-messenger synergy.

3.1. *The transient sky observed with ASTENA*

The discovery of the Gravitational Wave (GW) event GW170817[12] and its electromagnetic counterpart GRB170817A[13–16] marked the birth of the multi-messenger study of the transient sky. In the near future, this plural effort will solve fundamental astrophysics and cosmological questions. Furthermore, it will boost the discovery of sources of known and unknown classes of transients. Short GRBs represent the main class of transient which has been already confirmed to be associated with powerful GW events.

Polarization level in the range 30 - 80% of the prompt emission of the GRBs has been claimed for a few dozens events (a summary of the properties of the events can be found in [17, 18]) but, due to the limited statistical significance of the results, their confirmation is not definitive. These uncertainties are mainly due to the lack of sensitivity of the instruments used as gamma-ray polarimeters. A significant detection could probe the geometry of the magnetic field and its intensity which are precious information for shedding light into the jet composition and dissipation mechanism. Thanks to its polarimetric capabilities, along with a large detection area and broad pass-band, the WFM-IS would be the ideal instrument to measure the degree of polarization of the prompt emission, to perform a detailed time-resolved study and to evaluate the dependence of the polarization degree with energy.

Instruments capable of measuring the electromagnetic counterpart of GW events have a crucial importance for different reasons. Firstly, they can independently confirm the astrophysical nature of a GW trigger, particularly for the faintest events. Furthermore, since present interferometers have large uncertainties in the sky localization, a high sensitive wide FoV instrument like the WFM-IS could provide the localization of the order of 1 arcmin with the possibility of performing followup

observation with a soft gamma-ray telescope with an unprecedented sensitivity and angular resolution as the NFT.

It must be mentioned that with the launch of the Laser Interferometer Space Antenna (LISA) a plethora of GW events from stellar mass BH binaries will be detected in the mHz regime with a sky localization of the order of 1 deg^2. Such detections will work as alert for the observation of the same events at higher frequencies weeks/months later (with an accuracy of the order of tens of seconds) from ground interferometers. Thanks to the large FoV and to the PSLA of the WFM-IS will be possible to point in advance the instrument for the detection of the prompt hard X-ray counterpart of the event as well as the detection of the delayed hard X-ray emission through the NFT.

After the discovery of the GRB afterglow, till now this emission has been observed almost in all energy bands from IR to the soft X-ray regime up to ~ 10 keV. Afterglow detection in the 0.1–10 GeV, in the sub-TeV (100–440 GeV) and in the TeV energy regions have been reported.[19,20] One of the most important open issues that have still to be settled is the afterglow emission in the sub-MeV/MeV region which is almost completely undetected except for some events detected above few tens of keV[21–23] This is mainly due to the low flux emitted in this energy band, joined with the lack of sensitivity for the present instrumentation. From the prompt emission detected with the WFM-IS and though a fast repointing it would be possible, thanks to the sensitivity of the NFT, to measure the hard x-ray afterglow as well as its polarization level.

3.2. *Nuclear astrophysics with ASTENA*

In spite of its importance for understanding the inner regions of the astrophysical sources emitting hard X and mainly gamma-rays, nuclear astrophysics is still a theoretical field and almost experimentally unexplored, mainly due to observational limits. The reason is that present instrumentation in the hard-X and gamma-ray regime has absent or crude imaging capability and low sensitivity, compared with instruments in other wavelengths. One of the most relevant open issues in astrophysics is the origin of the 511 keV positron annihilation line observed from the Galactic Center (GC). Discovered in the seventies[24] neither the origin of the gamma emission, nor the responsible for the positron production have been found. The 511 keV annihilation line still represents a puzzle mainly due to the limitation of both sensitivity and angular resolution of current instruments operative in the 0.5 MeV region. To date, the best mapping of the line was obtained through SPI on-board INTEGRAL.[25] A variety of potential astrophysical sources responsible of the 511 keV signal and/or of the production of the positrons have been proposed, including type Ia supernovae,[26] GRBs,[27] microquasars,[28] low-mass X-ray binaries,[29] and neutron star mergers.[30] The high number of X–ray sources in the GC suggests the possibility that the 511 keV line is due to the emission of a number of discrete - unresolved - sources. The detection of a transient 0.5 MeV emission from V404 Cygni[31] is in

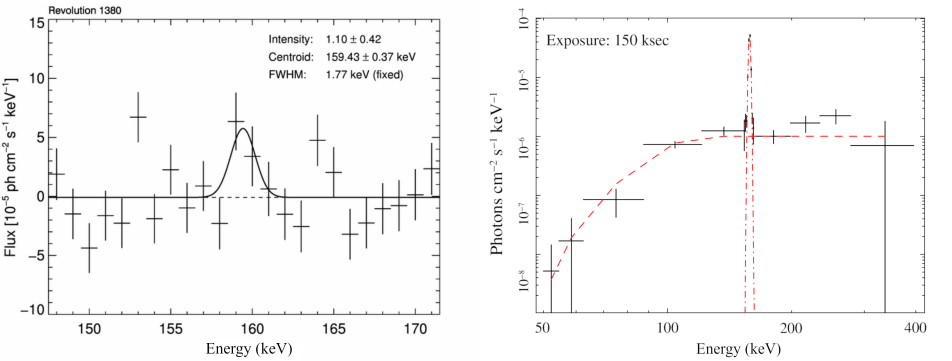

Fig. 7. Left: the 158 keV line due to the ^{56}Ni decay as observed from SN2014J as with the SPI on board INTEGRAL 3 weeks after the explosion. Reprinted from [9]. Right: the same line as observed with the NFT onboard ASTENA with 150 ks integration time. The simulated data (black points) consists of a continuum modeled with an absorbed power-law (red dashed line) with spectral index $\alpha = 0$ normalization 10^{-6} ph/cm^2/s @ 1 keV plus a Gaussian (red dot-dashed line) centered at 158 keV with σ=0.75 keV and normalization 1.1×10^{-4} ph/cm^2/s.

favour of this hypothesis. It is also believed that the 511 keV observed map would only represent the annihilation sites and not the positron sources. The propagation of the positrons away from the source could be the cause of a general broadening which originates the diffuse 511 keV emission. No point sources of annihilation radiation have yet been detected in the GC. Nevertheless, the angular resolution of INTEGRAL/SPI does not provide any definitive information about structure in the emission, even with several years of integrated data.[32] Under these considerations it is clear that observations of the GC with much higher angular resolution than that achievable with SPI aboard INTEGRAL together with high sensitive instruments are required in order to distinguish and localize - if any - discrete source of annihilation radiation.

Another topic under study that is worth to be mentioned is related to the nucleosynthesis of heavy elements in Type-Ia supernovae (SNe-Ia). Gamma-rays escaping the ejecta of SN-Ia can be used as tools for studying both the structure of the exploding star and the characteristics of the explosion. One of the key points is to estimate the amount of ^{56}Ni which is probably the most important physical parameter underlying the observed correlation of SNe-Ia luminosities with their light curves. The only direct way to estimate this amount is through the decay chain $^{56}\text{Ni} \rightarrow {}^{56}\text{Co} \rightarrow {}^{56}\text{Fe}$. The decay produces gamma-rays that ultimately power the optical light curve of the SN-Ia. Most models predict that the ejected material is not transparent to gamma-rays at least for tens of days since the explosion. As the ejecta proceeds, it becomes gradually more transparent to gamma-rays. Contrarily to the expectations, only two weeks after SN2014J through SPI/INTEGRAL observations, the characteristic gamma-ray lines 158 keV and 812 keV from the ^{56}Ni decay have been detected [9] and later confirmed at 5σ confidence level also with

ISGRI/INTEGRAL.[33] The early observations of gamma-rays from ^{56}Ni support the hypotesis of the presence of this element at the star surface. The intensity of the gamma-ray spectra mainly depends on the mass and distribution of the nickel mass. High sensitivity measurements focused at particular narrow lines would shed light on the SNe-Ia explosion mechanism and, ultimately to the correct distribution and mass of ^{56}Ni.

As an example of performances with ASTENA, in Fig. 7 we show the 158 keV line detected with SPI/INTEGRAL from SN2014J[9] for an exposure time of 150 ks. The estimated line intensity of $(1.1\pm 0.4) \times 10^{-4}$ ph/cm^2/s corresponds to a detection confidence level of 2.5σ. For comparison, with the same integration time, a spectrum consisting of a Gaussian profile (centroid energy 158 keV, $\sigma = 0.75$ keV) superposed to a continuum described by a power-law with spectra slope α=0 and normalization 10^{-6} ph/cm^2/s @ 1 keV has been simulated in order to estimate how it could be observed with the NFT aboard ASTENA. The same significance achieved by SPI in 150 ks is obtained in $\sim$1 ks.

4. Conclusions

Future missions for hard X-ray astrophysics require higher sensitivity than current instrumentation and capability of observing the sky in a broad energy pass-band. Such features will be crucial for solving some of the most important open issues. In addition, hard-X and soft gamma-ray polarimetry, which are still in their infancy, will play a crucial role in combination with spectroscopy, timing and imaging, providing information about the degree and the direction of polarization of the incident radiation. Particularly in hard X-rays, whose emission comes directly from the central engine of the sources, polarimetry is a powerful tool for investigating the magnetic field and the distribution of matter around astrophysical objects. Moreover, today hard X-/gamma-ray astrophysics suffers from the absence of devices that allow the radiation to be focused, the only method through which it is possible to increase the signal to noise of the observations and to suppress the instrumental background.

The ASTENA mission concept includes two complementary instruments through which it is possible to carry out both polarimetry and imaging in the hard X-ray regime. The WFM-IS is an array of 12 monitors that can effectively work in an unprecedented energy pass-band for a single instrument (2 keV - 20 MeV) thanks to the coupling of SDDs a and scintillator bars. Thanks to the adoption of a double scale coded mask, the instrument enables localization accuracy of about 1 arcmin and 5 arcmin in the energy pass-bands $<$ 30 keV and 30 - 150 keV, respectively. With this location accuracy, the WFM-IS is in complete synergy with the second instrument on board, the NFT: for the first time a focusing optics based on a Laue lens will be operative in a broad pass-band and with a FoV of a 4-5 arcminutes and an angular resolution of a few tens of arcseconds. Thanks to its focusing capability it provides an outstanding sensitivity for detecting source polarization[34] and both for

the continuum and for nuclear lines. The unprecedented broad pass band and the large FoV of the WFM-IS will allow to make surveys and to detect faint transient sources, including GRBs. The NFT, with its deep sensitivity for nearly on-axis sources, will be the ideal tool for followup observations of detected transient events.

In this work we have presented the ASTENA mission concept and details on both instruments aboard. We have described some key science issues that can be tackled with ASTENA as a stand-alone experiment and in synergy with other experiments, including its contribution to the multi-messenger astrophysics. We expect that a mission like ASTENA will be a breakthrough in general astrophysics and in particular for answering the questions that are still central in high energy astrophysics.

Acknowledgements

This work has been partially supported with the financial contribution from the ASI-INAF agreement n. 2017-14-H.0 "Studi per future missioni scientifiche", the ASI-INAF agreement n. 2018-10-H.1-2020 "HERMES Technologic Pathfinder", and the AHEAD EU Horizon 2020 project (Integrated Activities in the High Energy Astrophysics Domain), grant agreement n. 871158.

References

1. L. Piro, L. Natalucci and Ahead Consortium, AHEAD: Integrated Activities in the High Energy Astrophysics Domain, in *Exploring the Hot and Energetic Universe: The first scientific conference dedicated to the Athena X-ray observatory*.
2. L. Piro, The Activities for the High-Energy Astrophysics Domain (AHEAD), in *Whereabouts and Physics of the Roaming Baryons in the Universe*.
3. F. Favata, G. Hasinger, L. J. Tacconi, C. S. Arridge and K. S. O'Flaherty, Introducing the Voyage 2050 White Papers, contributions from the science community to ESA's long-term plan for the Scientific Programme, *Experimental Astronomy* **51**, 551 (June 2021).
4. F. Frontera, E. Virgilli, C. Guidorzi, P. Rosati, R. Diehl, T. Siegert, C. Fryer, L. Amati, N. Auricchio, R. Campana, E. Caroli, F. Fuschino, C. Labanti, M. Orlandini, E. Pian, J. B. Stephen, S. Del Sordo, C. Budtz-Jorgensen, I. Kuvvetli, S. Brandt, R. M. Curado da Silva, P. Laurent, E. Bozzo, P. Mazzali and M. Della Valle, Understanding the origin of the positron annihilation line and the physics of the supernova explosions, *White paper in response to Voyage 2050 long term planning of ESA science programme* **1**, p. 20 (Oct 2019).
5. C. Guidorzi, F. Frontera, G. Ghirlanda, G. stratta, C. Mundell, E. Virgilli, P. Rosati, E. Caroli, L. Amati, E. Pian, S. Kobayashi, G. Ghisellini, C. Fryer, M. Della Valle, E. Margutti, M. Marongiu, R. Martone, R. Campana, F. Fuschino, C. Labanti, M. Orlandini, J. B. Stephen, S. Brandt, R. M. Curado da Silva, L. P., M. R., E. Bozzo, R. Ciolfi, L. Burderi and T. Di Salvo, Deeper and broder: future observations in the X-/gamma-ray band of known and unknown, *White paper in response to Voyage 2050 long term planning pf ESA science programme* **1**, p. 20 (Oct 2019).
6. L. Amati, P. O'Brien, D. Götz, E. Bozzo, C. Tenzer *et al.*, The THESEUS space mission concept: science case, design and expected performances, *Advances in Space Research* **62**, 191 (July 2018).

7. G. K. Skinner and J. E. Grindlay, Coded masks with two spatial scales, *Astronomy and Astrophysics* **276**, p. 673 (September 1993).
8. G. Vedrenne, J. P. Roques, V. Schönfelder, P. Mandrou, G. G. Lichti, A. von Kienlin, B. Cordier, S. Schanne, J. Knödlseder, G. Skinner, P. Jean, F. Sanchez, P. Caraveo, B. Teegarden, P. von Ballmoos, L. Bouchet, P. Paul, J. Matteson, S. Boggs, C. Wunderer, P. Leleux, G. Weidenspointner, P. Durouchoux, R. Diehl, A. Strong, M. Cassé, M. A. Clair and Y. André, SPI: The spectrometer aboard INTEGRAL, *Astronomy and Astrophysics* **411**, L63 (November 2003).
9. R. Diehl, T. Siegert, W. Hillebrandt, S. A. Grebenev, J. Greiner, M. Krause, M. Kromer, K. Maeda, F. Röpke and S. Taubenberger, Early ^{56}Ni decay gamma rays from SN2014J suggest an unusual explosion, *Science* **345**, 1162 (September 2014).
10. F. Frontera, E. Virgilli, C. Guidorzi, P. Rosati, R. Diehl, T. Siegert, C. Fryer, L. Amati, N. Auricchio, R. Campana, E. Caroli, F. Fuschino, C. Labanti, M. Orlandini, E. Pian, J. B. Stephen, S. Del Sordo, C. Budtz-Jorgensen, I. Kuvvetli, S. Brandt, R. M. C. da Silva, P. Laurent, E. Bozzo, P. Mazzali and M. D. Valle, Understanding the origin of the positron annihilation line and the physics of supernova explosions, *Experimental Astronomy* **51**, 1175 (June 2021).
11. C. Guidorzi, F. Frontera, G. Ghirlanda, G. Stratta, C. G. Mundell, E. Virgilli, P. Rosati, E. Caroli, L. Amati, E. Pian, S. Kobayashi, G. Ghisellini, C. Fryer, M. D. Valle, R. Margutti, M. Marongiu, R. Martone, R. Campana, F. Fuschino, C. Labanti, M. Orlandini, J. B. Stephen, S. Brandt, R. C. d. Silva, P. Laurent, R. Mochkovitch, E. Bozzo, R. Ciolfi, L. Burderi and T. Di Salvo, A deep study of the high-energy transient sky, *Experimental Astronomy* **51**, 1203 (June 2021).
12. B. P. Abbott, LIGO Scientific Collaboration and Virgo Collaboration, GW170817: Observation of Gravitational Waves from a Binary Neutron Star Inspiral, *prl* **119**, p. 161101 (October 2017).
13. A. von Kienlin, C. Meegan and A. Goldstein, GRB 170817A: Fermi GBM detection., *GRB Coordinates Network* **21520**, p. 1 (January 2017).
14. V. Connaughton, GBM-LIGO Group, L. Blackburn, M. S. Briggs, J. Broida, E. Burns, J. Camp, T. Dal Canton, N. Christensen, A. Goldstein, R. Hamburg, C. M. Hui, P. Jenke, D. Kocevski, N. Leroy, T. Littenberg, J. McEnery, R. Preece, J. Racusin, P. Shawhan, K. Siellez, L. Singer, J. Veitch, P. Veres and C. Wilson-Hodge, LIGO/Virgo G298048: Fermi GBM trigger 170817.529 and LIGO single IFO trigger, *GRB Coordinates Network* **21506**, p. 1 (August 2017).
15. A. Goldstein, P. Veres, E. Burns, M. S. Briggs, R. Hamburg, D. Kocevski, C. A. Wilson-Hodge, R. D. Preece, S. Poolakkil, O. J. Roberts, C. M. Hui, V. Connaughton, J. Racusin, A. von Kienlin, T. Dal Canton, N. Christensen, T. Littenberg, K. Siellez, L. Blackburn, J. Broida, E. Bissaldi, W. H. Cleveland, M. H. Gibby, M. M. Giles, R. M. Kippen, S. McBreen, J. McEnery, C. A. Meegan, W. S. Paciesas and M. Stanbro, An Ordinary Short Gamma-Ray Burst with Extraordinary Implications: Fermi-GBM Detection of GRB 170817A, *ApJ Letter* **848**, p. L14 (October 2017).
16. V. Savchenko, C. Ferrigno, E. Kuulkers, A. Bazzano, E. Bozzo, S. Brandt, J. Chenevez, T. J. L. Courvoisier, R. Diehl, A. Domingo, L. Hanlon, E. Jourdain, A. von Kienlin, P. Laurent, F. Lebrun, A. Lutovinov, A. Martin-Carrillo, S. Mereghetti, L. Natalucci, J. Rodi, J. P. Roques, R. Sunyaev and P. Ubertini, INTEGRAL Detection of the First Prompt Gamma-Ray Signal Coincident with the Gravitational-wave Event GW170817, *ApJ Letter* **848**, p. L15 (October 2017).
17. M. L. McConnell, High energy polarimetry of prompt GRB emission, *New Astronomy Review* **76**, 1 (February 2017).

18. R. Gill, M. Kole and J. Granot, GRB Polarization: A Unique Probe of GRB Physics, *Galaxies* **9**, p. 82 (October 2021).
19. H. Abdalla, R. Adam, F. Aharonian, F. Ait Benkhali, E. O. Angüner, M. Arakawa, C. Arcaro, C. Armand, H. Ashkar, M. Backes, V. Barbosa Martins, M. Barnard, Y. Becherini, D. Berge, K. Bernlöhr, E. Bissaldi, R. Blackwell, M. Böttcher, C. Boisson, J. Bolmont, S. Bonnefoy, J. Bregeon, M. Breuhaus, F. Brun, P. Brun, M. Bryan, M. Büchele, T. Bulik, T. Bylund, M. Capasso, S. Caroff, A. Carosi, S. Casanova, M. Cerruti, T. Chand, S. Chandra, A. Chen, S. Colafrancesco, M. Curyło, I. D. Davids, C. Deil, J. Devin, P. deWilt, L. Dirson, A. Djannati-Ataï, A. Dmytriiev, A. Donath, V. Doroshenko, J. Dyks, K. Egberts, G. Emery, J. P. Ernenwein, S. Eschbach, K. Feijen, S. Fegan, A. Fiasson, G. Fontaine, S. Funk, M. Füßling, S. Gabici, Y. A. Gallant, F. Gaté, G. Giavitto, L. Giunti, D. Glawion, J. F. Glicenstein, D. Gottschall, M. H. Grondin, J. Hahn, M. Haupt, G. Heinzelmann, G. Henri, G. Hermann, J. A. Hinton, W. Hofmann, C. Hoischen, T. L. Holch, M. Holler, D. Horns, D. Huber, H. Iwasaki, M. Jamrozy, D. Jankowsky, F. Jankowsky, A. Jardin-Blicq, I. Jung-Richardt, M. A. Kastendieck, K. Katarzyński, M. Katsuragawa, U. Katz, D. Khangulyan, B. Khélifi, J. King, S. Klepser, W. Kluźniak, N. Komin, K. Kosack, D. Kostunin, M. Kreter, G. Lamanna, A. Lemière, M. Lemoine-Goumard, J. P. Lenain, E. Leser, C. Levy, T. Lohse, I. Lypova, J. Mackey, J. Majumdar, D. Malyshev, V. Marandon, A. Marcowith, A. Mares, C. Mariaud, G. Martí-Devesa, R. Marx, G. Maurin, P. J. Meintjes, A. M. W. Mitchell, R. Moderski, M. Mohamed, L. Mohrmann, C. Moore, E. Moulin, J. Muller, T. Murach, S. Nakashima, M. de Naurois, H. Ndiyavala, F. Niederwanger, J. Niemiec, L. Oakes, P. O'Brien, H. Odaka, S. Ohm, E. de Ona Wilhelmi, M. Ostrowski, I. Oya, M. Panter, R. D. Parsons, C. Perennes, P. O. Petrucci, B. Peyaud, Q. Piel, S. Pita, V. Poireau, A. Priyana Noel, D. A. Prokhorov, H. Prokoph, G. Pühlhofer, M. Punch, A. Quirrenbach, S. Raab, R. Rauth, A. Reimer, O. Reimer, Q. Remy, M. Renaud, F. Rieger, L. Rinchiuso, C. Romoli, G. Rowell, B. Rudak, E. Ruiz-Velasco, V. Sahakian, S. Sailer, S. Saito, D. A. Sanchez, A. Santangelo, M. Sasaki, R. Schlickeiser, F. Schüssler, A. Schulz, H. M. Schutte, U. Schwanke, S. Schwemmer, M. Seglar-Arroyo, M. Senniappan, A. S. Seyffert, N. Shafi, K. Shiningayamwe, R. Simoni, A. Sinha, H. Sol, A. Specovius, M. Spir-Jacob, Ł. Stawarz, R. Steenkamp, C. Stegmann, C. Steppa, T. Takahashi, T. Tavernier, A. M. Taylor, R. Terrier, D. Tiziani, M. Tluczykont, C. Trichard, M. Tsirou, N. Tsuji, R. Tuffs, Y. Uchiyama, D. J. van der Walt, C. van Eldik, C. van Rensburg, B. van Soelen, G. Vasileiadis, J. Veh, C. Venter, P. Vincent, J. Vink, H. J. Völk, T. Vuillaume, Z. Wadiasingh, S. J. Wagner, R. White, A. Wierzcholska, R. Yang, H. Yoneda, M. Zacharias, R. Zanin, A. A. Zdziarski, A. Zech, A. Ziegler, J. Zorn, N. Żywucka, F. de Palma, M. Axelsson and O. J. Roberts, A very-high-energy component deep in the gamma-ray burst afterglow, *Nature* **575**, 464 (November 2019).
20. MAGIC Collaboration, V. A. Acciari, S. Ansoldi, L. A. Antonelli, A. Arbet Engels, D. Baack, A. Babić, B. Banerjee, U. Barres de Almeida, J. A. Barrio, J. Becerra González, W. Bednarek, L. Bellizzi, E. Bernardini, A. Berti, J. Besenrieder, W. Bhattacharyya, C. Bigongiari, A. Biland, O. Blanch, G. Bonnoli, Ž. Bošnjak, G. Busetto, A. Carosi, R. Carosi, G. Ceribella, Y. Chai, A. Chilingaryan, S. Cikota, S. M. Colak, U. Colin, E. Colombo, J. L. Contreras, J. Cortina, S. Covino, G. D'Amico, V. D'Elia, P. da Vela, F. Dazzi, A. de Angelis, B. de Lotto, M. Delfino, J. Delgado, D. Depaoli, F. di Pierro, L. di Venere, E. Do Souto Espiñeira, D. Dominis Prester, A. Donini, D. Dorner, M. Doro, D. Elsaesser, V. Fallah Ramazani, A. Fattorini, A. Fernández-Barral, G. Ferrara, D. Fidalgo, L. Foffano, M. V. Fonseca, L. Font, C. Fruck, S. Fukami, S. Gallozzi, R. J. García López, M. Garczarczyk, S. Gasparyan, M. Gaug, N. Giglietto,

F. Giordano, N. Godinović, D. Green, D. Guberman, D. Hadasch, A. Hahn, J. Herrera, J. Hoang, D. Hrupec, M. Hütten, T. Inada, S. Inoue, K. Ishio, Y. Iwamura, L. Jouvin, D. Kerszberg, H. Kubo, J. Kushida, A. Lamastra, D. Lelas, F. Leone, E. Lindfors, S. Lombardi, F. Longo, M. López, R. López-Coto, A. López-Oramas, S. Loporchio, B. Machado de Oliveira Fraga, C. Maggio, P. Majumdar, M. Makariev, M. Mallamaci, G. Maneva, M. Manganaro, K. Mannheim, L. Maraschi, M. Mariotti, M. Martínez, S. Masuda, D. Mazin, S. Mićanović, D. Miceli, M. Minev, J. M. Miranda, R. Mirzoyan, E. Molina, A. Moralejo, D. Morcuende, V. Moreno, E. Moretti, P. Munar-Adrover, V. Neustroev, C. Nigro, K. Nilsson, D. Ninci, K. Nishijima, K. Noda, L. Nogués, M. Nöthe, S. Nozaki, S. Paiano, J. Palacio, M. Palatiello, D. Paneque, R. Paoletti, J. M. Paredes, P. Peñil, M. Peresano, M. Persic, P. G. Prada Moroni, E. Prandini, I. Puljak, W. Rhode, M. Ribó, J. Rico, C. Righi, A. Rugliancich, L. Saha, N. Sahakyan, T. Saito, S. Sakurai, K. Satalecka, K. Schmidt, T. Schweizer, J. Sitarek, I. Šnidarić, D. Sobczynska, A. Somero, A. Stamerra, D. Strom, M. Strzys, Y. Suda, T. Surić, M. Takahashi, F. Tavecchio, P. Temnikov, T. Terzić, M. Teshima, N. Torres-Albà, L. Tosti, S. Tsujimoto, V. Vagelli, J. van Scherpenberg, G. Vanzo, M. Vazquez Acosta, C. F. Vigorito, V. Vitale, I. Vovk, M. Will, D. Zarić and L. Nava, Teraelectronvolt emission from the gamma-ray burst GRB 190114C, *Nature* **575**, 455 (November 2019).

21. E. Maiorano, N. Masetti, E. Palazzi, F. Frontera, P. Grandi and et al., The puzzling case of GRB 990123: multiwavelength afterglow study, *Astronomy and Astrophysics* **438**, 821 (August 2005).
22. C. Kouveliotou, J. Granot, J. L. Racusin, E. Bellm, G. Vianello, S. Oates, C. L. Fryer, S. E. Boggs, F. E. Christensen, W. W. Craig, C. D. Dermer, N. Gehrels, C. J. Hailey, F. A. Harrison, A. Melandri, J. E. McEnery, C. G. Mundell, D. K. Stern, G. Tagliaferri and W. W. Zhang, NuSTAR Observations of GRB 130427A Establish a Single Component Synchrotron Afterglow Origin for the Late Optical to Multi-GeV Emission, *ApJ Letter* **779**, p. L1 (December 2013).
23. A. Martin-Carrillo, L. Hanlon, M. Topinka and et al., GRB 120711A: An intense INTEGRAL burst with long-lasting soft γ-ray emission and a powerful optical flash, *Astronomy and Astrophysics* **567**, p. A84 (Jul 2014).
24. I. Johnson, W. N. and R. C. Haymes, Detection of a Gamma-Ray Spectral Line from the Galactic-Center Region, *Astrophysical Journal* **184**, 103 (August 1973).
25. J. Knödlseder and GRI Consortium, GRI: The Gamma-Ray Imager Mission, in *The Obscured Universe. Proceedings of the VI INTEGRAL Workshop (2007)*,
26. E. Kalemci, S. E. Boggs, P. A. Milne and S. P. Reynolds, Searching for Annihilation Radiation from SN 1006 with SPI on INTEGRAL, *ApJ Letter* **640**, L55 (March 2006).
27. G. Bertone, A. Kusenko, S. Palomares-Ruiz, S. Pascoli and D. Semikoz, Gamma-ray bursts and the origin of galactic positrons, *Physics Letters B* **636**, 20 (April 2006).
28. N. Guessoum, P. Jean and N. Prantzos, Microquasars as sources of positron annihilation radiation, *Astronomy and Astrophysics* **457**, 753 (October 2006).
29. N. Prantzos, Astrophysical gamma-ray lines: A probe of stellar nucleosynthesis and star formation, in *5th INTEGRAL Workshop on the INTEGRAL Universe (2004)*,
30. R. Bartels, F. Calore, E. Storm and C. Weniger, Galactic binaries can explain the Fermi Galactic centre excess and 511 keV emission, *MNRAS* **480**, 3826 (November 2018).
31. T. Siegert, R. Diehl, J. Greiner, M. G. H. Krause, A. M. Beloborodov, M. C. Bel, F. Guglielmetti, J. Rodriguez, A. W. Strong and X. Zhang, Positron annihilation signatures associated with the outburst of the microquasar V404 Cygni, *Nature* **531**, 341 (March 2016).

32. L. Bouchet, J. P. Roques and E. Jourdain, On the Morphology of the Electron-Positron Annihilation Emission as Seen by Spi/integral, *Astrophysical Journal* **720**, 1772 (Sep 2010).
33. J. Isern, P. Jean, E. Bravo, J. Knödlseder and et al., Gamma-ray emission from SN2014J near maximum optical light, *Astrophysical Journal* **588**, p. A67 (Apr 2016).
34. M. Moita, M. Ferro, U. Frontera, O. Caroli, R. Virgilli, P. Stephen, F. Curado da Silva, P. Maia and A. Del Sordo, "Polarimetric prospects of a new hard X-/soft gamma-ray space mission for next decades", these proceedings.